Chapter 47
On the Use of a New Concept of Sampling Surfaces in Shell Theory

Gennady M. Kulikov and Svetlana V. Plotnikova

Abstract This paper focuses on the higher-order shell theory, which permits the use of 3D constitutive equations. It is based on the new concept of sampling surfaces (S-surfaces) inside the shell body. According to this concept, we introduce N not equally located S-surfaces parallel to the middle surface and choose displacements of these surfaces as fundamental shell unknowns. Such choice allows us to represent the higher-order shell formulation in a compact form and to derive strain-displacement equations, which are invariant under all rigid-body shell motions.

Keywords Higher-order shell theory · Sampling surface

47.1 Introduction

It is well-known that a conventional way for developing the higher-order shell theories accounting for thickness stretching is to utilize either quadratic or cubic series expansions in the thickness coordinate and to choose as unknowns the generalized displacements of the middle surface [1, 2]. In the present paper, we propose a new concept of S-surfaces inside the shell body. As S-surfaces Ω^1, Ω^2, ..., Ω^N, we choose outer surfaces and any inner surfaces inside the shell body and introduce displacement vectors $\mathbf{u}^1$, $\mathbf{u}^2$, ..., $\mathbf{u}^N$ of these surfaces as shell unknowns. Such choice of displacements with the consequent use of Lagrange polynomials of degree $N-1$ in the thickness direction permits one to derive strain-displacement equations, which precisely represent rigid-body shell motions in a convected curvilinear coordinate system. The latter is straightforward for development of the exact geometry (EG) solid-shell element formulation. The term "EG" reflects the fact that the parametrization of the reference surface is known and, therefore, the coefficients of the first and

G. M. Kulikov (✉) · S. V. Plotnikova
Tambov State Technical University, Sovetskaya Street, 106, Tambov 392000, Russia
e-mail: kulikov@apmath.tstu.ru

H. Altenbach and V.A. Eremeyev (eds.), *Shell-like Structures*,
Advanced Structured Materials 15, DOI: 10.1007/978-3-642-21855-2_47,

second fundamental forms of the reference surface can be taken exactly at each element node.

It should be mentioned that in recent works [3–5], the higher-order shell theories with three and four equally located S-surfaces have been developed. Herein, a general case with N not equally located S-surfaces is studied.

47.2 Kinematic Description of Undeformed Shell

Consider a thick shell of the thickness h. Let the midsurface Ω be described by orthogonal curvilinear coordinates θ_1 and θ_2, which are referred to the lines of principal curvatures of its surface. The coordinate θ_3 is oriented along the unit vector $\mathbf{e}_3$ normal to the reference surface Ω. Introduce the following notations: $\mathbf{r} = \mathbf{r}(\theta_1, \theta_2)$ is the position vector of any point of the midsurface; $\mathbf{a}_\alpha$ are the base vectors of the midsurface defined as

$$\mathbf{a}_\alpha = \mathbf{r}_{,\alpha} = A_\alpha \mathbf{e}_\alpha, \tag{47.1}$$

where $\mathbf{e}_\alpha$ are the orthonormal base vectors; A_α are the coefficients of the first fundamental form; $\mathbf{R} = \mathbf{r} + \theta_3 \mathbf{e}_3$ is the position vector of any point in the shell body; $\mathbf{R}^I = \mathbf{r} + \theta_3^I \mathbf{e}_3$ are the position vectors of S-surfaces; θ_3^I are the transverse coordinates of S-surfaces such that $\theta_3^1 = -h/2$ and $\theta_3^N = h/2$; $\mathbf{g}_i$ are the base vectors in the shell body given by

$$\mathbf{g}_\alpha = \mathbf{R}_{,\alpha} = A_\alpha c_\alpha \mathbf{e}_\alpha, \quad \mathbf{g}_3 = \mathbf{R}_{,3} = \mathbf{e}_3, \tag{47.2}$$

where $c_\alpha = 1 + k_\alpha \theta_3$ are the components of the shifter tensor; k_α are the principal curvatures of the midsurface; $\mathbf{g}_\alpha^I$ are the base vectors of S-surfaces (Fig. 47.1) defined as

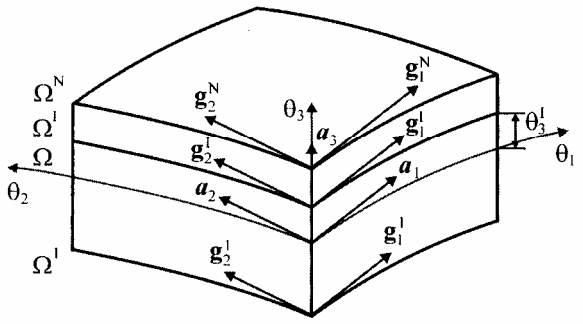

Fig. 47.1 Geometry of the shell

$$\mathbf{g}_\alpha^I = \mathbf{R}_{,\alpha}^I = A_\alpha c_\alpha^I \mathbf{e}_\alpha, \quad \mathbf{g}_3^I = \mathbf{e}_3, \tag{47.3}$$

where $c_\alpha^I = 1 + k_\alpha \theta_3^I$ are the components of the shifter tensor at S-surfaces.

Here and in the following developments, $(\ldots)_{,i}$ stands for the partial derivatives with respect to coordinates θ_i; Greek tensorial indices α, β range from 1 to 2; Latin tensorial indices i, j, k, m range from 1 to 3; indices I, J identify the belonging of any quantity to the S-surfaces and take values 1, 2, ..., N.

47.3 Kinematic Description of Deformed Shell

A position vector of the deformed shell is written as

$$\bar{\mathbf{R}} = \mathbf{R} + \mathbf{u}, \tag{47.4}$$

where $\mathbf{u}$ is the displacement vector, which is always measured in accordance with the total Lagrangian formulation from the initial configuration to the current configuration directly. In particular, the position vectors of S-surfaces are

$$\bar{\mathbf{R}}^I = \mathbf{R}^I + \mathbf{u}^I, \quad \mathbf{u}^I = \mathbf{u}(\theta_3^I), \tag{47.5}$$

where $\mathbf{u}^I(\theta_1, \theta_2)$ are the displacement vectors of S-surfaces.

The base vectors in the current shell configuration are defined as

$$\bar{\mathbf{g}}_i = \bar{\mathbf{R}}_{,i} = \mathbf{g}_i + \mathbf{u}_{,i}. \tag{47.6}$$

In particular, the base vectors of S-surfaces of the deformed shell (Fig. 47.2) are

$$\bar{\mathbf{g}}_\alpha^I = \bar{\mathbf{R}}_{,\alpha}^I = \mathbf{g}_\alpha^I + \mathbf{u}_{,\alpha}^I, \quad \bar{\mathbf{g}}_3^I = \bar{\mathbf{g}}_3(\theta_3^I) = \mathbf{e}_3 + \boldsymbol{\beta}^I, \tag{47.7}$$

$$\boldsymbol{\beta}^I = \mathbf{u}_{,3}(\theta_3^I), \tag{47.8}$$

where $\boldsymbol{\beta}^I(\theta_1, \theta_2)$ are the values of the derivative of the displacement vector with respect to coordinate θ_3 at S-surfaces.

The Green-Lagrange strain tensor can be expressed as

$$2\varepsilon_{ij} = \frac{1}{A_i A_j c_i c_j}(\bar{\mathbf{g}}_i \cdot \bar{\mathbf{g}}_j - \mathbf{g}_i \cdot \mathbf{g}_j), \tag{47.9}$$

where $A_3 = 1$ and $c_3 = 1$. In particular, the Green-Lagrange strain components at S-surfaces are

$$2\varepsilon_{ij}^I = 2\varepsilon_{ij}(\theta_3^I) = \frac{1}{A_i A_j c_i^I c_j^I}(\bar{\mathbf{g}}_i^I \cdot \bar{\mathbf{g}}_j^I - \mathbf{g}_i^I \cdot \mathbf{g}_j^I). \tag{47.10}$$

Substituting (47.3) and (47.7) into the strain-displacement relationships (47.10) and discarding non-linear terms, one derives

$$2\varepsilon_{\alpha\beta}^I = \frac{1}{A_\alpha c_\alpha^I}\mathbf{u}_{,\alpha}^I \cdot \mathbf{e}_\beta + \frac{1}{A_\beta c_\beta^I}\mathbf{u}_{,\beta}^I \cdot \mathbf{e}_\alpha,$$

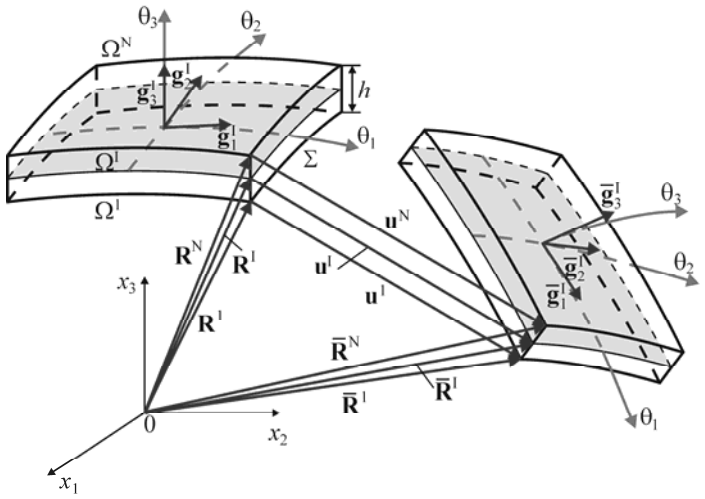

Fig. 47.2 Initial and current configurations of the shell

$$2\varepsilon^I_{\alpha 3} = \boldsymbol{\beta}^I \cdot \mathbf{e}_\alpha + \frac{1}{A_\alpha c^I_\alpha}\mathbf{u}^I_{,\alpha} \cdot \mathbf{e}_3, \quad \varepsilon^I_{33} = \boldsymbol{\beta}^I \cdot \mathbf{e}_3. \tag{47.11}$$

Next, we represent displacement vectors $\mathbf{u}^I$ and $\boldsymbol{\beta}^I$ in the reference surface frame $\mathbf{e}_i$ as follows:

$$\mathbf{u}^I = \sum_i u^I_i \mathbf{e}_i, \quad \boldsymbol{\beta}^I = \sum_i \beta^I_i \mathbf{e}_i. \tag{47.12}$$

Using (47.12) and presentations for the derivatives of unit vectors $\mathbf{e}_i$ with respect to orthogonal curvilinear coordinates

$$\frac{1}{A_\alpha}\mathbf{e}_{\alpha,\alpha} = -B_\alpha \mathbf{e}_\beta - k_\alpha \mathbf{e}_3, \quad \frac{1}{A_\alpha}\mathbf{e}_{\beta,\alpha} = B_\alpha \mathbf{e}_\alpha,$$

$$\frac{1}{A_\alpha}\mathbf{e}_{3,\alpha} = k_\alpha \mathbf{e}_\alpha, \quad B_\alpha = \frac{1}{A_\alpha A_\beta}A_{\alpha,\beta} \quad (\beta \neq \alpha), \tag{47.13}$$

one obtains

$$\frac{1}{A_\alpha}\mathbf{u}^I_{,\alpha} = \sum_i \lambda^I_{i\alpha}\mathbf{e}_i, \tag{47.14}$$

where

$$\lambda^I_{\alpha\alpha} = \frac{1}{A_\alpha}u^I_{\alpha,\alpha} + B_\alpha u^I_\beta + k_\alpha u^I_3, \quad \lambda^I_{\beta\alpha} = \frac{1}{A_\alpha}u^I_{\beta,\alpha} - B_\alpha u^I_\alpha \quad (\beta \neq \alpha),$$

$$\lambda^I_{3\alpha} = \frac{1}{A_\alpha}u^I_{3,\alpha} - k_\alpha u^I_\alpha. \tag{47.15}$$

Substituting (47.12) and (47.14) in strain-displacement relationships (47.11), we arrive at the index notations of these relationships

$$2\varepsilon^I_{\alpha\beta} = \frac{1}{c^I_\beta}\lambda^I_{\alpha\beta} + \frac{1}{c^I_\alpha}\lambda^I_{\beta\alpha},$$

$$2\varepsilon^I_{\alpha 3} = \beta^I_\alpha + \frac{1}{c^I_\alpha}\lambda^I_{3\alpha}, \quad \varepsilon^I_{33} = \beta^I_3. \tag{47.16}$$

Remark 1. The strain components (47.16) are objective, i.e., they represent precisely all rigid-body shell motions in any convected curvilinear coordinate system. It can be verified following a technique developed in [4, 5].

47.4 Displacement and Strain Approximations in Thickness Direction

Up to this moment, no assumptions concerning displacements and strains fields have been made. We start now with the first fundamental assumption of the proposed higher-order shell theory. Let us assume that the displacement field is approximated in the thickness direction according to the following law:

$$u_i = \sum_I L^I u^I_i, \tag{47.17}$$

where $L^I(\theta_3)$ are the Lagrange polynomials of degree $N-1$ expressed as

$$L^I = \prod_{J\neq I} \frac{\theta_3 - \theta^J_3}{\theta^I_3 - \theta^J_3} \tag{47.18}$$

such that $L^I(\theta^J_3) = 1$ for $J = I$ and $L^I(\theta^J_3) = 0$ for $J \neq I$.

The use of (47.8), (47.12) and (47.17) yields

$$\beta^I_i = \sum_J M^J(\theta^I_3) u^J_i, \tag{47.19}$$

where $M^I = L^I_{,3}$ are the derivatives of the Lagrange polynomials. Thus, the key functions β^I_i of the proposed higher-order shell theory are represented as a linear combination of displacements u^I_i.

The following step consists in a choice of correct approximation of strains through the thickness of the shell. It is apparent that the best solution of the problem is to choose the strain distribution, which is similar to the displacement distribution (47.10), that is,

$$\varepsilon_{ij} = \sum_I L^I \varepsilon^I_{ij}. \tag{47.20}$$

47.5 Variational Equation

Substituting strains (47.20) into the principal of the virtual work and introducing stress resultants

$$H_{ij}^I = \int_{-h/2}^{h/2} \sigma_{ij} L^I c_1 c_2 d\theta_3, \tag{47.21}$$

we arrive at the following variational equation:

$$\int\int_{\Omega} \left[\sum_I \sum_{i,j} H_{ij}^I \delta\varepsilon_{ij}^I - \sum_i \left(c_1^N c_2^N p_i^+ \delta u_i^N - c_1^1 c_2^1 p_i^- \delta u_i^1 \right) \right] A_1 A_2 d\theta_1 d\theta_2 = \delta W_\Sigma, \tag{47.22}$$

where p_i^-, p_i^+ are the surface loads acting on the bottom and top surfaces; W_Σ is the work done by external loads applied to the boundary surface Σ.

For simplicity, we restrict ourselves to the case of linear elastic materials. The natural choice for constitutive equations is the generalized Hook's law:

$$\sigma_{ij} = \sum_{k,m} C_{ijkm} \varepsilon_{km}. \tag{47.23}$$

Inserting stresses (47.23) in (47.21) and taking into account strain approximation (47.20), one finds

$$H_{ij}^I = \sum_J \sum_{k,m} D_{ijkm}^{IJ} \varepsilon_{km}^J, \tag{47.24}$$

where

$$D_{ijkm}^{IJ} = C_{ijkm} \int_{-h/2}^{h/2} L^I L^J c_1 c_2 d\theta_3. \tag{47.25}$$

Remark 2. Recalling that c_α are the polynomials of degree one, whereas L^I and L^J are the polynomials of degree $N-1$, one can carry out the exact integration in (47.25) by using the n-point Gaussian quadrature rule with $n = N+1$.

47.6 Finite Element Formulation

Variational equation (47.22) in conjunction with (47.24) and (47.25) is the basis for developing the EG four-node solid-shell element. The abbreviation EG is explained in Introduction. The finite element formulation is based on the simple and efficient interpolation of shells via curved EG four-node solid-shell elements

$$u_i^I = \sum_r N_r u_{ir}^I, \tag{47.26}$$

where $N_r(\xi_1, \xi_2)$ are the bilinear shape functions of the element; u^I_{ir} are the displacements of S-surfaces at element nodes; $\xi_\alpha = (\theta_\alpha - c_\alpha)/\ell_\alpha$ are the normalized curvilinear coordinates (Fig. 47.3); c_α are the coordinates of the element center; $2\ell_\alpha$ are the lengths of the element; the index r runs from 1 to 4 and denotes the number of nodes.

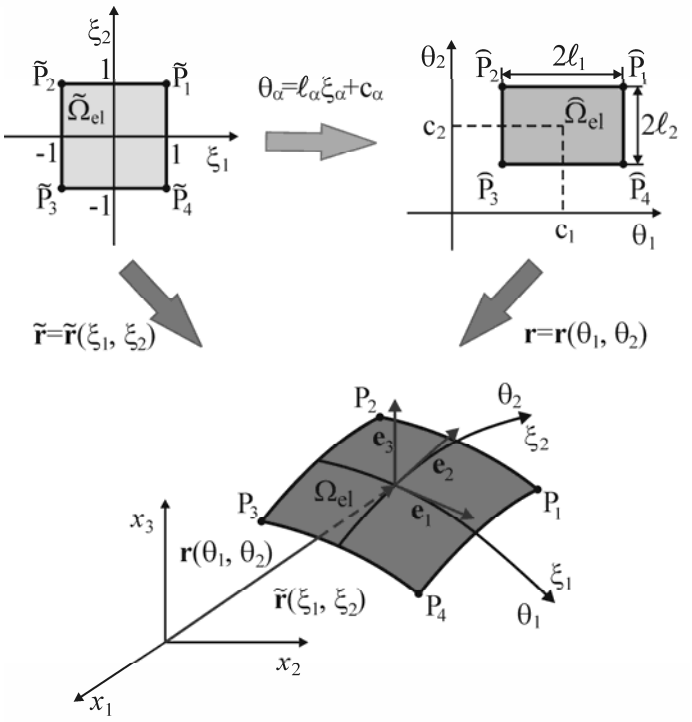

Fig. 47.3 Biunit square in (ξ_1, ξ_2)-space mapped into the EG four-node shell element in (x_1, x_2, x_3)-space

To implement the analytical integration throughout the element [6], we employ the assumed interpolation of strain components

$$\varepsilon^I_{ij} = \sum_r N_r \varepsilon^I_{ijr}, \quad \varepsilon^I_{ijr} = \varepsilon^I_{ij}(\tilde{P}_r), \tag{47.27}$$

where $\tilde{P}_r$ are the element nodes in (ξ_1, ξ_2)-space. The main idea of such approach can be traced back to the ANS method [7]. It is important to note that herein we treat the term "ANS" in a broader sense. In the proposed EG solid-shell element formulation, all strain components are assumed to vary bilinearly inside the biunit square. This implies that instead of expected non-linear interpolation of strains throughout the element the more suitable bilinear ANS interpolation is utilized.

Introducing a displacement vector of the shell element

$$\mathbf{U} = \left[\mathbf{U}_1^{\mathrm{T}} \mathbf{U}_2^{\mathrm{T}} \mathbf{U}_3^{\mathrm{T}} \mathbf{U}_4^{\mathrm{T}}\right]^{\mathrm{T}},$$

$$\mathbf{U}_r = \left[u_{1r}^1 u_{2r}^1 u_{3r}^1 u_{1r}^2 u_{2r}^2 u_{3r}^2 \ldots u_{1r}^N u_{2r}^N u_{3r}^N\right]^{\mathrm{T}} \tag{47.28}$$

and utilizing a standard finite element technique, one arrives at the element equilibrium equations

$$\mathbf{KU} = \mathbf{F}, \tag{47.29}$$

where $\mathbf{K}$ is the element stiffness matrix; $\mathbf{F}$ is the force vector.

47.7 Numerical Examples

The performance of the higher-order shell theory and EG four-node solid-shell element formulation developed is evaluated by using several exact solutions of the 3D elasticity theory extracted from the literature.

47.7.1 Square Plate Under Sinusoidal Loading

Consider first a simply supported square plate (Fig. 47.4) subjected to the sinusoidally distributed pressure load $p_3^- = -p_0 \sin\frac{\pi\theta_1}{a} \sin\frac{\pi\theta_2}{b}$. The mechanical and geometrical parameters are taken as follows: $E = 10^7$, $\nu = 0.3$ and $a = b = 1$. To compare the results derived with an exact solution [8], the following dimensionless variables are introduced:

$$U_3 = 100Eh^3 u_3(a/2, a/2, z)/p_0 a^4, \quad S_{11} = 10h^2\sigma_{11}(a/2, a/2, z)/p_0 a^2,$$

$$S_{12} = 10h^2\sigma_{12}(0, 0, z)/p_0 a^2, \quad S_{13} = 10h\sigma_{13}(0, a/2, z)/p_0 a,$$

$$S_{33} = \sigma_{33}(a/2, a/2, z)/p_0, \quad z = \theta_3/h.$$

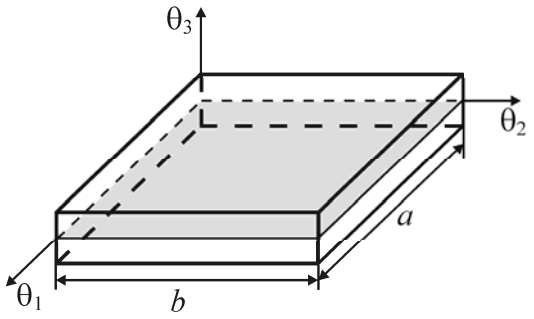

Fig. 47.4 Simply supported square plate

Owing to symmetry of the problem, only one quarter of the plate is modeled by the 64×64 mesh of EG four-node solid-shell elements. The data listed in Tables 47.1 and 47.2 show that the S-surfaces concept developed permits one to find the numerically exact solutions even for very thick plates. Fig. 47.5 presents the distribution of stresses in the thickness direction in the case of using seven equally located S-surfaces for different values of the slenderness ratio a/h. These results demonstrate the high potential of the proposed higher-order shell theory. This is due to the fact that the boundary conditions for transverse stresses S_{13} and S_{33} on the bottom and top surfaces are satisfied properly.

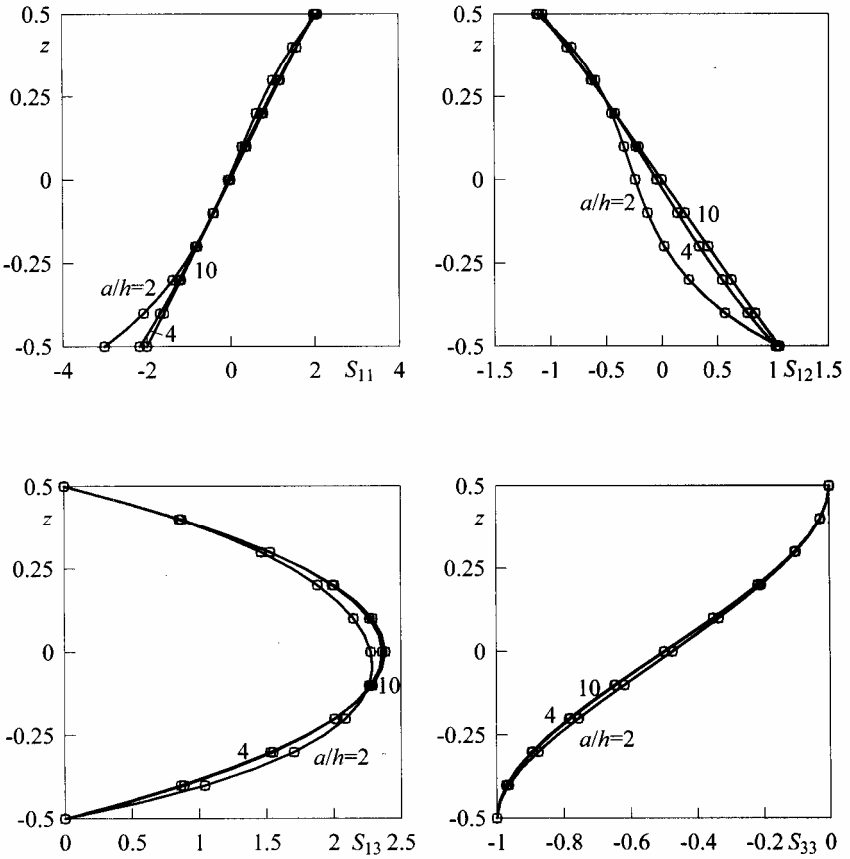

Fig. 47.5 Distribution of stresses S_{11}, S_{12}, S_{13} and S_{33} through the thickness of the plate for $N = 7$

Table 47.1 Results for a thick square plate with $a/h = 2$

Variant	$U_3(0)$	$S_{11}(-0.5)$	$S_{12}(-0.5)$	$S_{13}(0)$	$S_{33}(-0.5)$
$N = 3$	5.610	-2.683	0.830	1.596	-1.066
$N = 5$	6.042	-3.027	1.045	2.306	-1.013
$N = 7$	6.046	-3.013	1.045	2.276	-1.000
$N = 9$	6.046	-3.013	1.045	2.277	-1.000
Exact [8]	6.047	-3.014	1.046	2.277	-1.000

Table 47.2 Results for thick and thin square plates with five equally located S-surfaces

	$N = 5$				Exact solution [8]			
a/h	$U_3(0)$	$S_{11}(-0.5)$	$S_{12}(-0.5)$	$S_{13}(0)$	$U_3(0)$	$S_{11}(-0.5)$	$S_{12}(-0.5)$	$S_{13}(0)$
4	3.663	-2.174	1.026	2.369	3.663	-2.175	1.027	2.362
10	2.942	-2.004	1.056	2.384	2.942	-2.004	1.056	2.383
100	2.804	-1.975	1.063	2.387	2.804	-1.976	1.064	2.387

47.7.2 Cylindrical Shell Under Sinusoidal Loading

Next, we study a simply supported cylindrical shell with $L/R = 4$ subjected to the sinusoidal loading $p_3^- = -p_0 \sin\frac{\pi\theta_1}{L}\cos 4\theta_2$, where θ_1 and θ_2 are the longitudinal and circumferential coordinates of the midsurface; L and R are the length and radius of the shell. The shell is made of the unidirectional composite with the fibers oriented in the circumferential direction. The mechanical parameters are taken as follows:

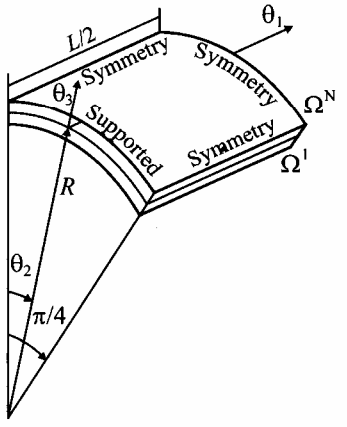

Fig. 47.6 Simply supported cylindrical shell

Table 47.3 Results for a thick cylindrical shell with $R/h = 2$

Variant	$U_3(0)$	$S_{11}(0.5)$	$S_{22}(0.5)$	$S_{12}(-0.5)$	$S_{13}(0)$	$S_{23}(0)$	$S_{33}(0)$
$N = 3$	6.693	1.151	1.433	-0.962	0.993	-1.674	-0.4216
$N = 5$	7.248	0.936	4.410	-1.582	1.508	-2.123	-0.3762
$N = 7$	7.466	1.201	5.061	-1.729	1.495	-1.981	-0.3649
$N = 9$	7.497	1.353	5.162	-1.755	1.497	-2.063	-0.3755
Exact [9]	7.503	1.332	5.163	-1.761	1.504	-2.056	-0.37

Table 47.4 Results for thick and thin shells with seven equally located S-surfaces

	$N = 7$				Exact solution [9]			
R/h	$U_3(0)$	$S_{22}(0.5)$	$S_{13}(0)$	$S_{23}(0)$	$U_3(0)$	$S_{22}(0.5)$	$S_{13}(0)$	$S_{23}(0)$
4	2.782	4.854	0.9863	-2.970	2.783	4.859	0.987	-2.990
10	0.9188	4.048	0.5199	-3.665	0.9189	4.051	0.520	-3.669
100	0.5169	3.840	0.3927	-3.856	0.5170	3.843	0.393	-3.859

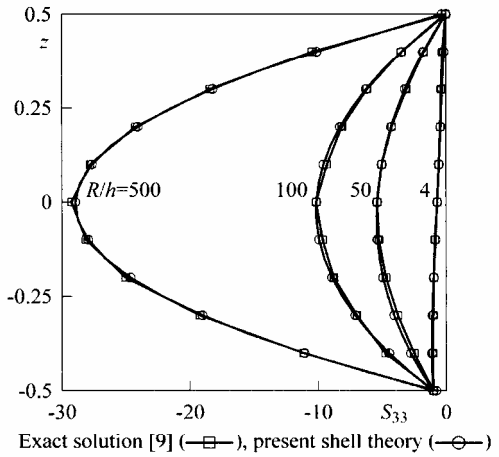

Fig. 47.7 Distribution of transverse normal stresses S_{33} through the thickness of the shell for $N = 7$

$E_L = 25E_T$, $G_{LT} = 0.5E_T$, $G_{TT} = 0.2E_T$, $E_T = 10^6$, $\nu_{LT} = \nu_{TT} = 0.25$. Here, subscripts L and T refer to the fiber and transverse directions of the ply. To compare the derived results with the exact solution [9] the following dimensionless variables are utilized:

$$S_{11} = 100h^2\sigma_{11}(L/2, 0, z)/p_0R^2, \quad S_{22} = 10h^2\sigma_{22}(L/2, 0, z)/p_0R^2,$$

$$S_{12} = 100h^2\sigma_{12}(0, \pi/8, z)/p_0R^2, \quad S_{13} = 100h\sigma_{13}(0, 0, z)/p_0R,$$

$$S_{23} = 10h\sigma_{23}(L/2, \pi/8, z)/p_0R, \quad S_{33} = \sigma_{33}(L/2, 0, z)/p_0,$$
$$U_3 = 10E_L h^3 u_3(L/2, 0, z)/p_0R^4, \quad z = \theta_3/h.$$

Due to symmetry of the problem, only one sixteenth of the shell (Fig. 47.6) is discretized with the 32×128 mesh of EG four-node solid-shell elements. The data listed in Tables 47.3 and 47.4 demonstrate again the high potential of the shell theory developed. Additionally, Fig. 47.7 presents the distribution of transverse normal stresses in the thickness direction in the case of using seven equally located S-surfaces for different values of the slenderness ratio R/h. It is seen that boundary conditions on the outer surfaces are satisfied correctly.

47.8 Conclusions

A simple and efficient concept of S-surfaces inside the shell body has been proposed. This concept permits the use of 3D constitutive equations and leads for the sufficient number of S-surfaces to the numerically exact solutions of 3D elasticity problems for thick and thin shells.

Acknowledgements This work was supported by Russian Ministry of Education and Science (Grant No 2.1.1/10003) and Russian Foundation for Basic Research (Grant No 08–01–0373).

References

1. Noor AK, Burton WS (1990) Assessment of computational models for multilayered composite shells. Appl Mech Rev 43:67–97
2. Carrera E (2002) Theories and finite elements for multilayered, anisotropic, composite plates and shells. Arch Comp Meth Eng 9:1–60
3. Kulikov GM (2001) Refined global approximation theory of multilayered plates and shells. J Eng Mech 127:119–125
4. Kulikov GM, Plotnikova SV (2008) Finite rotation geometrically exact four-node solid-shell element with seven displacement degrees of freedom. Comp Model Eng Sci 28:15–38
5. Kulikov GM, Carrera E (2008) Finite deformation higher-order shell models and rigid-body motions. Int J Solids Struct 45:3153-3172
6. Kulikov GM, Plotnikova SV (2006) Geometrically exact assumed stress-strain multilayered solid-shell elements based on the 3D analytical integration. Comp Struct 84:1275-1287
7. Bathe KJ, Dvorkin EN (1986) A formulation of general shell elements - the use of mixed interpolation of tensorial components. Int J Num Meth Eng 22:697-722
8. Vlasov BF (1957) On the bending of rectangular thick plate. Trans Moscow State Univ 2:25-31 (in Russian)
9. Varadan TK, Bhaskar K (1991) Bending of laminated orthotropic cylindrical shells – an elasticity approach. Comp Struct 17:141-156